

# ATIC, PAMELA, HESS, Fermi and nearby Dark Matter subhalos

Michael Kuhlen\*

*Institute for Advanced Study, Einstein Drive, Princeton, NJ 08540*

Dmitry Malyshev†

*CCPP, 4 Washington Place, Meyer Hall of Physics, NYU, New York, NY 10003*

(Dated: October 29, 2018)

We study the local flux of electrons and positrons from annihilating Dark Matter (DM), and investigate how its spectrum depends on the choice of DM model and inhomogeneities in the DM distribution. Below a cutoff energy, the flux is expected to have a universal power-law form with an index  $n \approx -2$ . The cutoff energy and the behavior of the flux near the cutoff is model dependent. The dependence on the DM host halo profile may be significant at energies  $E < 100$  GeV and leads to softening of the flux,  $n < -2$ . There may be additional features at high energies due to the presence of local clumps of DM, especially for models in which the Sommerfeld effect boosts subhalo luminosities. In general, the flux from a nearby clump gives rise to a harder spectrum of electrons and positrons, with an index  $n > -2$ . Using the *Via Lactea II* simulation, we estimate the probability of such subhalo effects in a generic Sommerfeld-enhanced model to be at least 4%, and possibly as high as 15% if subhalos below the simulation's resolution limit are accounted for. We discuss the consequences of these results for the interpretation of the ATIC, PAMELA, HESS, and Fermi data, as well as for future experiments.

PACS numbers: 95.35.+d, 96.50.S-, 98.70.Sa

## Contents

## References

15

<b>I. Introduction</b>	2
<b>II. Propagation of electrons</b>	3
<b>III. Dark Matter in a Host Halo</b>	4
A. Sommerfeld enhancement	4
B. DM model dependence	6
C. Profile dependence	6
<b>IV. Clumps of Dark Matter</b>	7
A. Via Lactea subhalos	7
B. The flux from a local clump	9
<b>V. Conclusions</b>	13

---

\*Electronic address: mqk@ias.edu

†Electronic address: dm137@nyu.edu; On leave of absence from ITEP, Moscow, Russia, B. Chermushkinskaya 25

## I. INTRODUCTION

One of the corner stones of the standard big bang cosmology is the presence of dark matter (DM). Although DM comprises at least 80% of all matter in the Universe, surprisingly little is known about its nature. A recent rise of interest in the DM problem has been triggered by observations of anomalies in several high energy cosmic ray experiments. The PAMELA Collaboration [1] reported an increasing positron fraction in the energy range 10 - 100 GeV, while the ATIC [2], PPB-BETS [3], and HESS [4] experiments suggest a bump in the total  $e^+e^-$  flux between 100 GeV and 1 TeV. Recent Fermi/LAT [5] and HESS [6] data show a smooth spectrum which is harder than the expected background at energies  $E > 100$  GeV and has a break around 1 TeV but without significant bumps.

The possibility that the anomalies are due to annihilating or decaying DM is very exciting, although standard astrophysical sources, such as pulsars or nearby supernova remnants [7, 8, 9, 10, 11, 12, 13, 14, 15, 16], provide a viable explanation as well.

In order for DM annihilation to produce the necessary  $e^+e^-$  flux, the cross section must be 100 - 1000 times larger than the standard value ( $\langle\sigma v\rangle \sim 3 \times 10^{-26} \text{ cm}^3 \text{ s}^{-1}$ ) inferred from the relic DM abundance. Boosts due to DM inhomogeneities are expected to be  $\lesssim 10$  [17] in the solar neighborhood, and an additional mechanism, such as the Sommerfeld enhancement, is necessary [18, 19, 20]. The Sommerfeld enhancement can be further amplified in subhalos due to their lower velocity dispersions [21]. DM models, proposed to explain the ATIC and PAMELA anomalies, include the lightest supersymmetric particles [22, 23, 24, 25, 26, 27], Kaluza-Klein particles [28, 29, 30], and various phenomenological scenarios [31, 32, 33, 34, 35, 36, 37] (for a recent review see, e.g., [38, 39])

In the presence of a large number of competing possibilities, one of the most important questions is what properties of the  $e^+e^-$  flux are model dependent and what properties are universal. In this work we study the dependence of the  $e^+e^-$  flux on

- the shape of DM host halo, and
- the presence of subhalos.

The dependence on DM models and on the host halo density profile was recently investigated in [31, 40, 41, 42]. One may notice that the flux is nearly independent of the density profile and that the choice of DM model seems to affect the spectral shape only at high energies near the break.

We show that for any DM model there exists an energy  $E_* \lesssim M_{\text{DM}}$  such that the  $e^+e^-$  flux has a universal behavior  $F_{e^\pm}(E) \sim E^{-2}$  for energies  $1 \text{ GeV} \ll E \ll E_*$ . In general, for  $E \ll E_*$ , the index depends on the energy loss function,  $\dot{E} = -b(E)$ , for electrons propagating in the interstellar medium (ISM)

$$F_{e^\pm} \sim \frac{1}{b(E)} \quad E \ll E_*, \quad (1)$$

where  $b(E) \sim E^2$  for  $E \gg 1 \text{ GeV}$ . The behavior in Eq. (1) does not depend on the DM model, but the value of  $E_*$  is model dependent. Eq. (1) may be also modified at energies  $E \sim 10 \text{ GeV}$  due to a dependence on the DM density profile.

This paper is organized as follows: In Sec. II, we review the propagation of electrons and positrons in the ISM and derive Eq. (1). In Sec. III, we study the dependence of the spectral index on DM models and on the spatial distribution of the DM. For our purposes, the most important difference between DM models is the number of steps in the annihilation-decay process, with more decay steps leading to a softer  $e^+e^-$  injection spectrum. However, propagation effects then ensure that the final spectrum exhibits the universal behavior of Eq. (1). Likewise, variations in the DM spatial distribution also do not change this behavior. As we show, the spectral slope is not affected by linear gradients in the source function, with the leading order correction arising from second derivatives. The Earth is sufficiently far from the Galactic center such that the corresponding effects are small, although the corrections may become important at  $E \sim 10 \text{ GeV}$  due to an increase in the characteristic diffusion distance.

A local clump of DM, on the other hand, may result in a significant variation in the spectral index.

- DM models,

In Sec. IV, we investigate this possibility using *Via Lactea II* (hereafter VL2), one of the highest resolution numerical simulations of the DM structure of a Milky-Way-scale halo [17, 43, 44]. We find that on average there is one  $M > 10^5 M_\odot$  clump within 3 kpc from Earth. Without Sommerfeld enhancement, the likelihood of boosting the local flux by a significant factor ( $>10$ ) due to one such nearby subhalo is very low, in agreement with previous findings [17, 45]. Allowing for Sommerfeld enhancement, however, the average luminosity from nearby clumps can match (or even exceed) the smooth host halo contribution. We show that, in general, the electron flux from a nearby DM clump is harder than from the host halo (as also observed in [45, 46, 47, 48]). In the DM annihilation picture, the high energy ( $\sim 600$  GeV) flux observed by ATIC, PPB-BETS, and HESS is consistent with being produced by a single DM clump, but in order to explain PAMELA the flux must be dominated by the smooth host halo below energies of  $\sim 100$  GeV (another possibility to explain PAMELA is via a second, more distant, large clump of DM as pointed out in [45]). Recent Fermi and HESS data are significantly smoother than the ATIC data and are fitted better with the flux from the host halo without contributions from large subhalos. We conclude in Sec. V by summarizing which properties of the  $e^+e^-$  flux are model dependent and which are universal.

## II. PROPAGATION OF ELECTRONS

The propagation of electrons in the ISM is described by diffusion in the Galactic magnetic field and energy losses [49, 50]. At energies  $E > 10$  GeV, the main losses are from synchrotron radiation and inverse Compton scattering, which can be estimated as

$$\dot{E} = -b_0 E^2, \quad (2)$$

where  $b_0 = 1.6 \times 10^{-16} \text{ GeV}^{-1} \text{ s}^{-1}$  for the local densities of starlight, infrared, and CMB photons [51] and a magnetic field of  $3 \mu\text{G}$  [50]. For relativistic electrons, the diffusion coefficient can be expressed as

$$D(E) = D_0 \left( \frac{E}{1 \text{ GeV}} \right)^\delta. \quad (3)$$

In the examples, we will use  $D_0 = 20 \text{ pc}^2 \text{ kyr}^{-1}$  and  $\delta = 0.6$  [52, 53, 54]. We will also assume that the diffusion zone in the vertical direction (away from the Galactic plane) is sufficiently large,  $L \gtrsim 4$  kpc, such that the escape of electrons from the Galaxy can be neglected. Models with a small diffusion zone,  $L \lesssim 1$  kpc, tend to have exponential suppression of the flux from DM at energies  $E \lesssim 100$  GeV [40], which would contradict the PAMELA data. Our main qualitative conclusions will not depend on the choice of parameters  $b_0$ ,  $D_0$ , and  $\delta$ . As a useful simplification, we will also assume that these parameters do not depend on  $\mathbf{x}$ .

The electron energy spectrum  $f = \frac{dN}{dE dV}$  evolves according to the diffusion-loss equation [49, 50]

$$\frac{\partial f}{\partial t} = \frac{\partial}{\partial E} (b(E)f) + D(E)\nabla^2 f + Q(\mathbf{x}, E, t). \quad (4)$$

The general solution of this equation is found in [49, 55]. If the source is constant in time, then  $\partial f/\partial t = 0$  and the equation simplifies to the usual diffusion equation. If we introduce a new variable  $\lambda(E)$  such that

$$\frac{d\lambda}{dE} = -\frac{D(E)}{b(E)}, \quad (5)$$

then

$$\frac{\partial (bf)}{\partial \lambda} - \nabla^2 (bf) = \frac{b(E)}{D(E)} Q(\mathbf{x}, E). \quad (6)$$

The Green's function for the diffusion equation is

$$G(\mathbf{x}, \lambda) = \frac{1}{(4\pi\lambda)^{3/2}} e^{-\frac{\mathbf{x}^2}{4\lambda}}, \quad (7)$$

and so the general solution to Eq. (6) is given by

$$f(\mathbf{x}, E) = \frac{1}{b(E)} \int d^3x_0 \int_E^\infty dE_0 G(\mathbf{x} - \mathbf{x}_0, \lambda(E, E_0)) \cdot Q(\mathbf{x}_0, E_0), \quad (8)$$

where

$$\lambda(E, E_0) = \int_E^{E_0} \frac{D(E') dE'}{b(E')}. \quad (9)$$

Our approximation is valid if the characteristic propagation distance,  $x^2 = 6\lambda(E, E_0)|_{E_0 \rightarrow \infty}$ , is much smaller

than the size of the vertical diffusion zone  $L$ . For our choice of parameters, this gives

$$E \gtrsim \left(60 \frac{\text{kpc}^2}{L^2}\right)^{\frac{1}{1-\delta}} \text{ GeV} \quad (10)$$

If  $L \sim 4$  kpc, then  $E \gtrsim 30$  GeV. For smaller energies there is an exponential suppression due to escape of electrons from the Galaxy.

For a homogeneous monochromatic source  $Q(\mathbf{x}_0, E_0) = Q_0 \delta(E - M_{\text{DM}})$ , the solution to Eq. (8) is

$$f(E) = \frac{Q_0}{b(E)}, \quad (11)$$

which has the behavior (1) announced in the Introduction. For energies  $E \gg 1$  GeV,  $b(E) \sim E^2$  (cf. Eq. (2)) and therefore  $f(E) \sim E^{-2}$ . One of the main purposes of the paper is to elucidate how the index  $n = -2$  changes for different DM models and different DM distributions.

### III. DARK MATTER IN A HOST HALO

The source function of electrons and positrons coming from annihilating DM is

$$Q(\mathbf{x}, E) = \frac{1}{2} \frac{\rho_{\text{DM}}^2}{M_{\text{DM}}^2} \langle \sigma v \rangle \frac{dN_{\text{ann}}}{dE}, \quad (12)$$

where  $\frac{\rho_{\text{DM}}}{M_{\text{DM}}}$  is the DM number density,  $\langle \sigma v \rangle$  is the thermally averaged annihilation cross-section, and  $dN_{\text{ann}}/dE$  is the differential energy spectrum of electrons and positrons produced in a single annihilation event. Here we assume that the DM particle is its own antiparticle, e.g., a Majorana fermion, otherwise there is an additional factor of  $1/2$ .

As we discuss in more detail below, the cross section may exhibit a velocity dependent boost factor  $\langle \sigma v \rangle = \langle \sigma v \rangle_0 S(v)$ , where  $\langle \sigma v \rangle_0$  is the cross section at freeze-out and  $\lim_{v \rightarrow c} S = 1$ . Generically, this enhancement scales as  $S \sim 1/v$ , although resonances exist for certain parameter choices, in which case  $S \sim 1/v^2$  [19]. Note that in either case the boost saturates at small velocities.

DM halos in general are not isothermal and have lower velocity dispersions, and hence higher boost factors, in their centers [56, 57, 58]. Given a density profile, and assuming equilibrium and spherical symmetry, it is straightforward to solve the Jeans' equation for the corresponding velocity dispersion profile  $\sigma_v(r)$ . For a Navarro, Frenk, and White (NFW) density profile, the resulting velocity dispersions peak at about the scale radius and decrease towards the center as  $\sigma_v(r) \sim r^{1/2}$  [59]. This is a limiting case [60], and all other profiles (e.g. the Einasto profile) have shallower velocity dispersion profiles.

The source function (12) can be split into a product of  $\mathbf{x}$ -dependent and  $E$ -dependent functions

$$Q(\mathbf{x}, E) = \kappa L(\mathbf{x}) Q(E), \quad (13)$$

where

$$\kappa = \frac{\langle \sigma v \rangle_0}{2M_{\text{DM}}^2}. \quad (14)$$

The  $\mathbf{x}$ -dependent part is the luminosity

$$L(\mathbf{x}) = \rho_{\text{DM}}^2(\mathbf{x}) S(v(\mathbf{x})), \quad (15)$$

and the  $E$ -dependent part is the injection spectrum

$$Q(E) = \frac{dN_{\text{ann}}}{dE}(E), \quad (16)$$

where we choose the normalization such that  $\int_0^\infty Q(E) dE$  is the total average number of electrons and positrons produced in an annihilation.

#### A. Sommerfeld enhancement

In the following we will assume the standard DM density  $\rho_{\text{DM}} = 0.3 \text{ GeV cm}^{-3}$  and a freeze-out cross section  $\langle \sigma v \rangle_0 = 3 \times 10^{-26} \text{ cm}^3 \text{ s}^{-1}$ . This cross section is too small to give a sufficient annihilation rate for the PAMELA and ATIC anomalies, and hence a boost factor of 100 - 1000 is necessary. Recent Fermi data are consistent with this conclusion. If we assume that the PAMELA anomaly is due to dark matter, then the absence of steplike features in Fermi data below the cutoff requires  $M_{\text{DM}} \gtrsim 1 \text{ TeV}$ . Consequently the same boost factor 100 - 1000 is required to explain PAMELA.

An elegant way to increase the annihilation cross section without affecting the relic abundance, is to assume the existence of a new light force carrier  $\phi$  in the dark sector,  $m_\phi \sim \mathcal{O}(\text{GeV})$ . This additional force results in a Sommerfeld enhancement [18], which is unimportant at freeze-out when particles are close to relativistic, but can significantly boost annihilation rates today. There may be further enhancement, if the annihilation proceeds through the formation of WIMPonium [61], a meta-stable bound state of two DM particles. This process is analogous to the annihilation of electrons and positrons through positronium, which is dominant at low velocities. For some parameters in the DM sector, it is possible to radiatively create WIMPonium by emitting a  $\phi$  particle, and in this case the WIMPonium annihilation channel dominates over immediate annihilation.

We now demonstrate that in every model with parameters that do not allow for WIMPonium creation, there exists an upper bound,

$$S \lesssim \frac{2\pi}{\sqrt{v}}, \quad (17)$$

on the nonresonant boost factor, where  $v$  is the relative velocity of the particles.

Generic (nonresonant) Sommerfeld enhancement is [18]

$$S(v) = \frac{\pi\alpha}{v}. \quad (18)$$

This enhancement factor saturates when the deBroglie wavelength of the DM particles becomes equal to the force range  $\frac{1}{M_{\text{DM}}v} \sim \frac{1}{m_\phi}$ , thus

$$S \lesssim \frac{\pi\alpha M_{\text{DM}}}{m_\phi}. \quad (19)$$

WIMPonium cannot be created if the corresponding binding energy is smaller than the mass of the mediator

$$\frac{1}{4}\alpha^2 M_{\text{DM}} \lesssim m_\phi. \quad (20)$$

Collecting these pieces together, we find

$$\frac{\pi\alpha}{v} \lesssim \frac{\pi\alpha M_{\text{DM}}}{m_\phi} \lesssim \frac{4\pi}{\alpha}, \quad (21)$$

and thus

$$\alpha \lesssim 2\sqrt{v}, \quad (22)$$

which gives the bound (17). In any particular model the precise value of the numeric coefficient in (17) may be different, but the parametric form should be the same (unless there are some additional reasons that prevent WIMPonium creation).

At the location of the Sun (8 kpc), the velocity dispersion of the DM particles is  $\sigma_v \approx 200$  km/s [21]. Taking this as a proxy for the relative velocities of annihilating DM particles, we find

$$S(200 \text{ km/s}) \lesssim 250. \quad (23)$$

Thus, the local Sommerfeld enhancement,  $S(200 \text{ km/s})$ , cannot exceed  $\sim 250$  without taking into account WIMPonium creation or resonance effects. If we allow for WIMPonium creation ( $m_\phi < 1/4\alpha^2 M_{\text{DM}}$ ), then the annihilation cross section increases by an additional factor of 7 (3) for fermionic (bosonic) DM particles [61], i.e., for fermionic DM particles the enhancement factor is

$$S(v) \approx 20\frac{\alpha}{v}. \quad (24)$$

In order to parameterize the Sommerfeld enhancement as a function of velocity, we need to specify the normalization  $S_0$  and the saturation velocity  $v_{\text{min}}$ . Then, for small velocities ( $v \ll \alpha$ ),

$$S(v) = S_0 \frac{v_0}{v + v_{\text{min}}}. \quad (25)$$

We take  $v_0$  to be the local velocity dispersion,  $v_0 = 200$  km/s. In the examples we discuss below, we set  $v_{\text{min}} = 3$  km/s and  $S_0 = 600$ . These parameters are rather generic and can be obtained, for instance, in a fermionic DM model with a vector boson mediator with  $\alpha = 1/50$  and  $m_\phi/M_{\text{DM}} = 10^{-5}$ . The small mass ratio is necessary to have a small saturation velocity,  $\frac{v_{\text{min}}}{c} \sim \frac{m_\phi}{M_{\text{DM}}}$ . For small  $v_{\text{min}}$  the role of small subhalos is greater since their velocity dispersion is smaller. For larger  $v_{\text{min}}$  the luminosity of small subhalos becomes smaller and the probability to have an observable effect is reduced.

For  $M_{\text{DM}} \sim 1$  TeV we have  $m_\phi \sim 10$  MeV  $> 2m_{e^\pm}$ , i.e. this model is kinematically viable. In building a realistic model, one has to check various constraints from diffuse gamma rays and neutrino fluxes [41, 42,

62, 63, 64]. However, instead of trying to find a specific model that satisfies all current observational data, we now discuss some general properties of the  $e^+e^-$  flux from annihilating DM.

### B. DM model dependence

For a homogeneous monochromatic source, the electron spectrum was derived in Eq. (11). In general, the spectrum can be approximated as  $f \sim E^n$  with an energy dependent index  $n(E)$ . Since at low energies we expect  $f(E) \sim 1/b(E)$ , the variation of the index will be defined as

$$\delta n \equiv \frac{d \log b(E) f(E)}{d \log E}. \quad (26)$$

For a homogeneous source, the electron density is

$$f(E) = \frac{1}{b(E)} \int_E^{M_{\text{DM}}} Q(E_0) dE_0. \quad (27)$$

If the injection spectrum has the form of a power law

$$Q(E) \sim E^\alpha \quad \alpha > -1, \quad (28)$$

then the integral is saturated at  $E_0 \sim M_{\text{DM}}$  and the variation of  $n$  is small for  $E \ll M_{\text{DM}}$ .

We define the break energy  $E_*$  by the condition

$$\delta n(E_*) = -1. \quad (29)$$

The flux  $F_{e^\pm} \sim E^{-3}$  near  $E_*$ , which is approximately the same scaling as the backgrounds [2, 65]. Thus the ratio  $\frac{F_{e^\pm}}{F_{\text{backgr}}}$  is maximal near  $E_*$ .

As an example, we consider DM annihilation followed by a chain of  $(k-1)$  two-body decays

$$2\chi \rightarrow 2\phi_1 \rightarrow 4\phi_2 \rightarrow \dots \rightarrow 2^{k-1}e^+ + 2^{k-1}e^- \quad (30)$$

We assume that  $m_{i+1} \ll m_i$ , i.e. the decay products of  $\phi_i$  are relativistic in the rest frame of  $\phi_i$ . The spectrum of  $\phi_i$  particles is [42]

$$\begin{aligned} Q_1(E) &= 2\delta(M_\chi - E) \\ Q_i(E) &= \frac{2^i}{(i-2)!} \left(\log \frac{M_{\text{DM}}}{E}\right)^{i-2} \quad i > 1, \end{aligned} \quad (31)$$

where we include the multiplicity  $2^i$  in the definition of the source functions  $Q_i(E)$ .

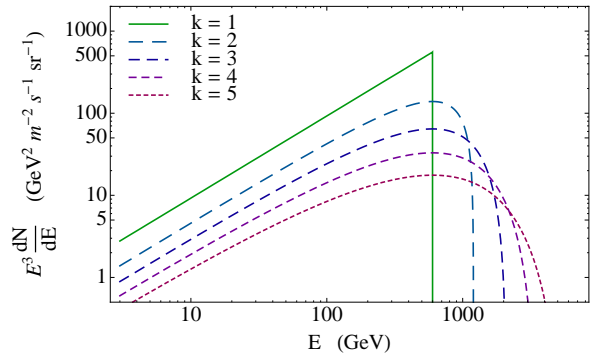


FIG. 1: The  $e^+e^-$  flux depending on the number of steps in the toy model DM annihilation (see text). In order to keep the maximum values of  $E^3 F$  at  $E_* = 600$  GeV, we choose the DM mass  $M_{\text{DM}} \sim e^{\frac{k-1}{2}} E_*$ . Apart from overall normalization, the spectra look similar to each other for  $E \ll E_*$ . Model dependence shows up for energies  $E \gtrsim E_*$ .

The DM particle mass is not directly observed, rather the experiments measure the peak of the bump, i.e.  $E_*$ , which is a function of  $M_{\text{DM}}$ . Motivated by the ATIC data we fix  $E_* = 600$  GeV and find the necessary  $M_{\text{DM}}$  in order to satisfy condition (29)

$$\begin{aligned} \frac{M_{\text{DM}}}{E_*} &= 1, 2, 3.5, 6, 10 \dots \\ k &= 1, 2, 3, 4, 5 \dots \end{aligned} \quad (32)$$

For large  $k$ , the ratio grows exponentially,  $\frac{M_{\text{DM}}}{E_*} \approx e^{\frac{k-1}{2}}$ . The corresponding fluxes for  $k \leq 5$  are shown in Fig. 1. At energies  $E \ll 600$  GeV the spectra look very similar to each other, indicating model independence. At higher energies, on the other hand, the spectral shape is sensitive to the value of  $k$ , i.e. it depends on the DM model.

### C. Profile dependence

In this section we calculate the variation of the index due to a coordinate dependence of the luminosity. In order to find the spectrum of electrons coming from DM annihilating in the host halo, we take the source function (13) and substitute it in Eq. (8). At the

observer's position  $\mathbf{x} = 0$ , we get

$$b(E)f(E) = \int_E^\infty dE_0 \kappa Q(E_0) \cdot \int d^3x_0 \frac{1}{(4\pi\lambda)^{3/2}} e^{-\frac{x_0^2}{4\lambda}} L(\mathbf{x}_0) \quad (33)$$

In the previous section we considered the variation of the index due to the lower limit of the  $E_0$  integration. Now the integral over  $x_0$  is a function of  $\lambda(E, E_0)$  and this introduces an additional  $E$  dependence.

The resulting variation is

$$\delta n \sim \frac{d \log \lambda}{d \log E} \frac{\langle \frac{x^2}{2\lambda} L \rangle - 3 \langle L \rangle}{\langle L \rangle}, \quad (34)$$

where  $\frac{d \log \lambda}{d \log E} \sim (\delta - 1)$  and the average of a function  $f(x)$  is defined as

$$\langle f \rangle = \int d^3x \frac{1}{(4\pi\lambda)^{3/2}} e^{-\frac{x^2}{4\lambda}} f(x). \quad (35)$$

In particular,  $\langle \mathbf{x}^2 \rangle = 6\lambda$ . Thus, for a uniform source,  $\delta n = 0$ . For a linear gradient  $\delta L = b_i x^i$ ,  $\langle \delta L \rangle = \langle \frac{x^2}{2\lambda} \delta L \rangle = 0$ . Consequently, the first correction to  $n$  follows from the second derivative of  $L(\mathbf{x})$ .

For slowly varying  $L(\mathbf{x})$ ,

$$\delta n \sim -(1 - \delta) \lambda \frac{\nabla^2 L}{L}. \quad (36)$$

At the position of the Earth, the luminosity can be approximated as

$$L(r) = \rho_{\text{DM}}^2 S \sim r^{-\alpha}. \quad (37)$$

Consequently

$$\nabla^2 L(r) = \frac{1}{r^2} \partial_r r^2 \partial_r (\rho_{\text{DM}}^2 S) \sim \frac{\alpha(\alpha - 1)}{r^2} L(r). \quad (38)$$

Substituting this expression in Eq. (36), we get

$$\delta n \sim -(1 - \delta) \alpha (\alpha - 1) \frac{\lambda}{r_0^2}, \quad (39)$$

where  $r_0 \approx 8$  kpc is the distance from the center of the Galaxy to Earth. Since  $\lambda \ll r_0^2$ , this variation is generally small (Fig. 2).

The situation is different when the density inhomogeneity is due to a discrete subhalo. For a DM clump with size  $l_{\text{cl}} \ll \sqrt{\lambda}$  we can neglect the first term in the

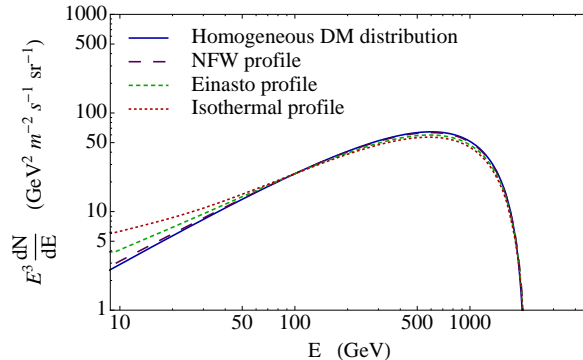


FIG. 2: The dependence of  $e^+e^-$  flux on the DM halo profile. We use NFW [66], Einasto ( $\alpha = 0.17$ ) [67], and Isothermal [68, 69] profiles. The difference from the homogeneous distribution is proportional to  $x_{\text{diff}}^2(E)/r_0^2$ , where  $r_0 = 8$  kpc is the distance from the center of the Galaxy. For small energies the characteristic diffusion distance increases and the corrections are more significant. Similar results were obtained in [70] for  $M_{\text{DM}} = 300$  GeV.

numerator of Eq. (34). The correction to the index then becomes positive and  $\mathcal{O}(1)$ ,  $\delta n \sim -\frac{d \log \lambda}{d \log E} \approx (1 - \delta)$ . This leads to a harder electron spectrum, and the index is no longer independent of the DM model and the properties of ISM. We consider some examples in the next section.

#### IV. CLUMPS OF DARK MATTER

In this section, we describe the properties of subhalos using the results of the *Via Lactea II* (VL2) simulation and study their influence on the electron flux spectrum.

##### A. Via Lactea subhalos

With a particle mass of  $4000 M_\odot$ , VL2 can resolve subhalos down to  $\sim 10^5 M_\odot$ . For our purposes, the important subhalo properties are their size, their number density, and their luminosity. Since the annihilation rate scales as  $\rho^2 S$ , it is strongly peaked toward the centers of subhalos. For an NFW profile,  $\sim 90\%$  of the total annihilation luminosity originates from within

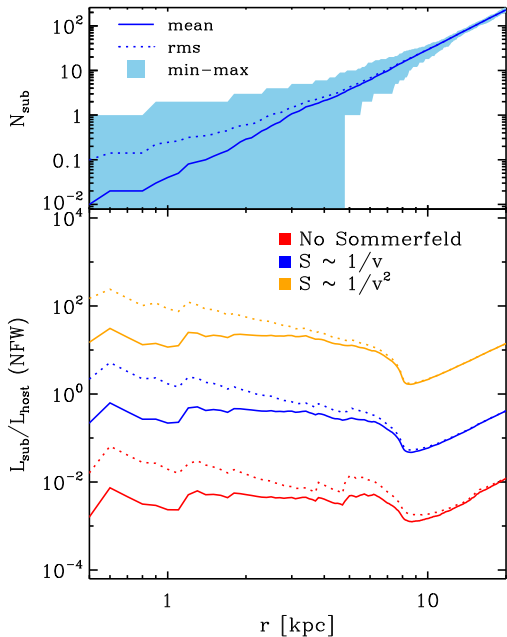


FIG. 3: Some properties of DM subhalos using results of *Via Lactea II* simulation [17]. The upper plot shows the expected number of subhalos within a distance  $r$  from the Earth. In the lower plot we show the ratio of luminosities of all subhalos within  $r$  to the total luminosity of the host halo in the solid sphere of radius  $r$  around the Earth. We plot the ratio of luminosities without Sommerfeld enhancement, with generic  $S \sim 1/v$  enhancement, and with resonant  $S \sim 1/v^2$  enhancement. These curves only account for subhalos resolved in the *Via Lactea II* simulation,  $M_{\text{sub}} \gtrsim 10^5 M_{\odot}$ , and should be viewed as lower limits.

the scale radius, which is much smaller than the typical propagation distance of  $\sim 1$  kpc. Consequently, we will treat the subhalos as point sources.

We determined the properties of the local subhalo population from the simulation by randomly placing 100 sample spheres of radius 20 kpc, each at a distance of 8 kpc from the host halo center. For each sample sphere, we identified all subhalos whose centers fall within the sphere. The top panel of Fig. 3 shows the mean, root mean square, minimum, and maximum number of subhalos over the ensemble, as a function of radius within the sample sphere. To a good approximation the mean number of subhalos grows as  $r^3$ , and

hence we will assume that the subhalo number density is constant. On average there is one subhalo within  $r \approx 3$  kpc. Note that these results refer solely to the portion of the substructure hierarchy that is resolved in the VL2 simulation, i.e.  $M_{\text{sub}} > 10^5 M_{\odot}$ . The subhalo mass function has been measured in simulations to be a simple power law  $dn/dM \sim M^{-\alpha}$  over 4 - 5 decades of subhalo mass [17, 71], with a logarithmic slope  $\alpha \approx 1.9$  independent of distance from the host halo center. This implies that the local density of subhalos with mass larger than  $M$  may be extrapolated to  $M < 10^5 M_{\odot}$  as

$$n_{\text{sub}}(M) \approx 9 \times 10^{-3} \text{ kpc}^{-3} \left( \frac{M}{10^5 M_{\odot}} \right)^{-0.9}. \quad (40)$$

In the bottom panel of Fig. 3 we plot the mean and the root mean square of  $L_{\text{sub}}/L_{\text{host}}$ , the ratio of the luminosity from all VL2-resolved subhalos to the smooth host halo luminosity, as a function of the enclosed radius within the sample spheres. We assigned a luminosity to each subhalo by assuming NFW density and velocity dispersion profiles that are matched to the values of  $V_{\text{max}}$  and  $r_{V_{\text{max}}}$  as measured in the VL2 simulation.  $V_{\text{max}}$  is the peak of the circular velocity curve  $v_c^2(r) = GM(< r)/r$ , and  $r_{V_{\text{max}}}$  is the radius at which this peak occurs, and both quantities are robustly determined in the numerical simulation. We have checked that our results do not change qualitatively if an Einasto profile is assumed instead.

We compare three different models: one with  $S = 1$  (no Sommerfeld enhancement), one with  $S \sim 1/v$ , and one with  $S \sim 1/v^2$ . Without Sommerfeld enhancement, the average contribution to the total luminosity from  $M > 10^5 M_{\odot}$  subhalos is negligible, in agreement with previous findings [45]. In the  $S \sim 1/v$  model, however, this subhalo contribution is already as large as that from the smooth host halo, and in the  $S \sim 1/v^2$  case it dominates by close to 2 orders of magnitude. We caution that these are ensemble averaged ratios: even at a distance of 3 kpc only 70% of the sample spheres contain one or more  $M > 10^5 M_{\odot}$  subhalo, and at 2 (1) kpc this fraction drops to 24% (3%). The situation for models with Sommerfeld enhancement can be summarized as follows:



- i) when one or more  $M > 10^5 M_\odot$  subhalos happen to lie within the electron diffusion region, their combined flux dominates that of the smooth host halo;
- ii) the probability of finding one or more such subhalos remains below 50% out to 2.6 kpc, and a mean occupancy of one such subhalo is reached only at 3 kpc;
- iii) the ensemble averaged expectation value of  $L_{\text{sub}}/L_{\text{host}}$  is unity for  $1/v$  models ( $M > 10^5 M_\odot$  subhalos are about as important as the host halo) and  $\sim 100$  for  $1/v^2$  models ( $M > 10^5 M_\odot$  subhalos are much more important than the host halo).

These results suggest that if a model relies on the Sommerfeld effect to explain the high energy cosmic ray anomalies, then there is a non-negligible probability of an individual DM subhalo affecting the high energy electron flux.

We stress once more that these results refer merely to the subhalos resolved in VL2. In the cold dark matter picture of structure formation, the clumping of DM should continue far beyond the artificial resolution limit of current state-of-the-art numerical simulations like VL2. The total luminosity from all subhalos below the simulation's resolution limit may very well dominate the local pair production rate from DM annihilation, if the dense cores of such low mass subhalos are able to withstand the disruptive forces from tidal interactions with the DM host halo and with stars and molecular clouds in the Galactic disk [72]. However, the diffusive nature of the electron propagation would average out the contribution from subhalos with an  $\mathcal{O}(1)$  probability of lying within the diffusion distance of  $\sim 1$  kpc, rendering their contribution indistinguishable from the homogeneous host halo source. Let us define the characteristic mass scale  $M_1$  such that

$$\frac{4\pi}{3} x_{\text{diff}}^3 \int_{M_1}^{\infty} dn_{\text{sub}} = 1. \quad (41)$$

where  $x_{\text{diff}} \sim 1$  kpc in our case. For the local subhalo abundance of Eq. (40),  $M_1 = 2,600 M_\odot$ . Any additional features in the electron spectrum from annihilating DM must arise from a small number of large subhalos,  $M > M_1$ , within the diffusion region.

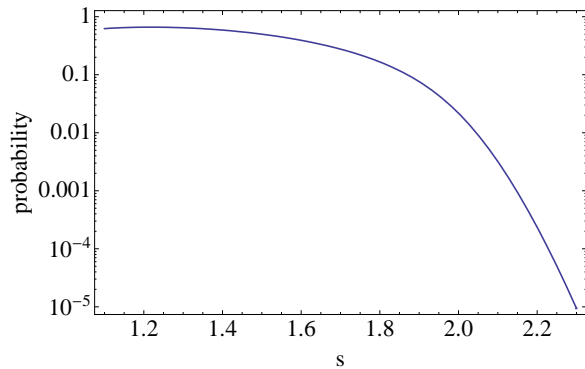


FIG. 4: The probability to observe an order one feature at high energies from a clump of dark matter versus the index  $s$  of the luminosity function [Eq. (42)]. The break at  $s = 2$  corresponds to equipartition of DM luminosity. For  $s < 2$  the luminosity is saturated by large clumps, for  $s > 2$  the luminosity is saturated by small clumps. The overall normalization is model dependent.

## B. The flux from a local clump

In this section we study an example of the flux from a single DM subhalo in an  $S \sim 1/v$  model and compare it with the flux from the host halo.

At first, let us estimate the probability to see a feature from a single DM clump relative to the flux from the host halo and the averaged flux from minihalos (defined to have  $M < M_1$ ). Effectively, the answer to this question depends on only one parameter, the logarithmic scaling  $s$  of the subhalo number density with respect to the luminosity

$$\frac{dn_{\text{sub}}}{dL} \sim L^{-s}. \quad (42)$$

Qualitatively, if  $s > 2$  then the integrated luminosity is saturated by small clumps and the probability to have a significant flux from a large clump is negligible. If  $s < 2$ , then the luminosity is saturated by the large clumps and the probability to see an additional feature is significant.

Let us estimate the probability of an  $\mathcal{O}(1)$  feature for the equipartition distribution,  $s = 2$ . In this case  $n_{\text{sub}}(L) \sim L^{-1}$ , i.e. subhalos with 10 times larger luminosity have 10 times smaller density. Denote by  $L_1$

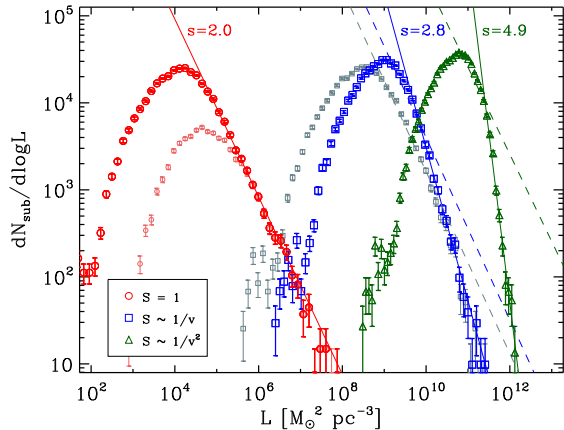


FIG. 5: The luminosity function from VL2 subhalos, assuming NFW density and velocity dispersion profiles for the same three models as in Fig. 3. Without Sommerfeld enhancement (circles) the luminosity function is equipartitioned ( $s = 2$ ) down to the simulation’s completeness limit,  $L \sim 10^4 M_\odot^2 \text{pc}^{-3}$ . For comparison we also show the distribution when the sample is restricted to subhalos with more than 250 particles ( $M > 10^6 M_\odot$ ) [small circles]. In the  $S \sim 1/v$  Sommerfeld case (squares), the luminosity function is steeper ( $s = 2.8$ ) above the saturation luminosity of  $L_{\text{sat}} \sim 2 \times 10^9 M_\odot^2 \text{pc}^{-3}$ . Below saturation the distribution is expected to flatten to  $s = 2$  (dashed lines), and indeed this behavior is clearly seen for a model with a higher saturation luminosity of  $L_{\text{sat}} \sim 3 \times 10^{10} M_\odot^2 \text{pc}^{-3}$  corresponding to  $m_\phi/M_{\text{DM}} = 5 \times 10^{-5}$  (small squares). For  $S \sim 1/v^2$  (triangles) the luminosity function above  $L_{\text{sat}} = 10^{11} M_\odot^2 \text{pc}^{-3}$  is even steeper ( $s = 4.9$ ).

the luminosity corresponding to a subhalo of mass  $M_1$ . Suppose that there are  $p$  decades of subhalos below  $M_1 \sim 10^3 M_\odot$ , which in the equipartition case each contribute an equal amount to the total luminosity. For a minimum DM clump mass of  $10^{-12} - 10^{-4} M_\odot$  [73, 74] we can roughly estimate  $p = 7 - 15$ .

The total luminosity of subhalos with  $L < L_1$  is then  $L_{\text{minihalos}} = pL_1$ . For the purpose of estimation, suppose that the luminosity of the host halo is smaller than  $L_{\text{minihalos}}$ ; then we should expect to observe an  $\mathcal{O}(1)$  feature if there is a subhalo with luminosity  $L_p = pL_1$  within the diffusion distance. The probability of such

a subhalo is

$$\pi_p \sim \frac{n_{\text{sub}}(L_p)}{n_{\text{sub}}(L_1)} = \frac{1}{p} \sim 0.1, \quad (43)$$

and is independent of the value of  $L_1$  and of the details of the propagation model.

For general  $s$ , the luminosity of a subhalo that is able to produce a significant feature is

$$\begin{aligned} L_p(s) &\sim \int_{L_{\text{min}}}^{L_1} dL L \frac{dn_{\text{sub}}}{dL} \\ &\sim \frac{s-1}{s-2} \left[ \left( \frac{L_1}{L_{\text{min}}} \right)^{s-2} - 1 \right] L_1. \end{aligned} \quad (44)$$

The luminosity  $L_1$  is defined as  $\frac{4\pi}{3} x_{\text{diff}}^3 \int_{L_1}^{\infty} dn_{\text{sub}} = 1$  and  $x_{\text{diff}} \sim 1 \text{ kpc}$  in our case. The corresponding density is

$$n_{\text{sub}}(L_p) \sim L_p^{1-s} \quad (45)$$

and the probability becomes

$$\pi(s) \sim \frac{n_{\text{sub}}(L_p)}{n_{\text{sub}}(L_1)} = \left( \frac{L_p(s)}{L_1} \right)^{1-s} \quad (46)$$

The normalization of this probability is model dependent. In particular, it depends on the ratio of the host halo luminosity to that in the subhalos. The shape of  $\pi(s)$ , however, is universal. It has a break at  $s = 2$  with a flat probability for luminosities saturated by large clumps,  $s < 2$ , and a rapidly decaying probability for luminosity saturated by small clumps,  $s > 2$ . The function  $\pi(s)$  for  $L_1/L_{\text{min}} \sim 10^{10}$  is presented in Fig. 4.

In Fig. 5 we show an empirical determination of the subhalo luminosity function  $dN_{\text{sub}}/dL$  from the VL2 subhalos for the same three models we considered in Fig. 3. As before, the subhalo luminosities are estimated using an NFW density and velocity dispersion profile, and we use the  $S \sim 1/v$  model normalized to  $S_0 = S(200 \text{ km/s}) = 600$ . We include all subhalos within the host’s virial radius  $r_{200} = 402 \text{ kpc}$ . In the case without Sommerfeld enhancement we find  $s = 2$  (equipartition) down to the luminosity completeness limit of  $L \sim 10^4 M_\odot^2 \text{pc}^{-3}$ . The turnover at smaller luminosities is due to the fact that we do not resolve

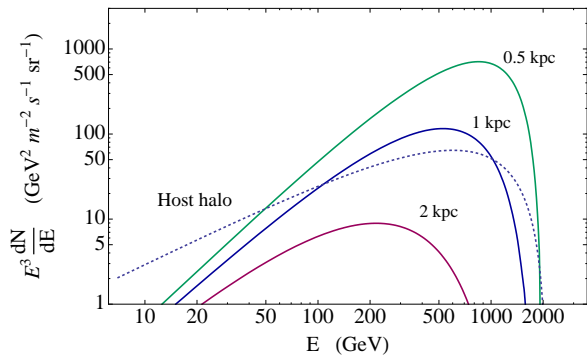


FIG. 6: The flux of electrons from a typical DM subhalo at distances  $r = 0.5, 1, 2$  kpc from Earth versus the flux from the DM annihilation in the host halo. The flux from a subhalo is significant for  $r \lesssim 1$  kpc and the corresponding spectrum is harder than the spectrum from the host halo. We use  $S \sim 1/v$  Sommerfeld enhancement of annihilation,  $M_{\text{DM}} = 2.1$  TeV,  $m_\phi/M_{\text{DM}} = 10^{-5}$ ,  $\alpha = 1/50$ , and  $S_0 = 600$ . The subhalo luminosity is given in Eq. (47).

halos with  $M < 10^5 M_\odot$  and correspondingly low luminosities. When only subhalos with more than 250 particles ( $M > 10^6 M_\odot$ ) are included, then the distribution departs from a power law at roughly 10 times higher luminosities.

The Sommerfeld-enhanced luminosity functions are steeper, with  $s = 2.8$  for  $S \sim 1/v$ , and  $s = 4.9$  for the  $S \sim 1/v^2$  model. In the smallest mass subhalos resolved in VL2, the internal velocity dispersions become comparable to the saturation velocity. Even smaller subhalos will be fully saturated, and the slope of their luminosity function should be identical to the non-Sommerfeld-enhanced case. We thus expect a break in the power law right around the saturation luminosity  $L_{\text{sat}}$ . We estimate  $L_{\text{sat}}$  by determining the mean luminosity of all subhalos with  $V_{\text{max}}/c$  within 10% of  $v_{\text{min}}/c = m_\phi/M_{\text{DM}} = 10^{-5}$ , and find  $L_{\text{sat}} = 2 \times 10^9 M_\odot^2 \text{pc}^{-3}$  for  $S \sim 1/v$  and  $L_{\text{sat}} = 10^{11} M_\odot^2 \text{pc}^{-3}$  for  $S \sim 1/v^2$ . Since these values are very close to the VL2 completeness limit, it is difficult to clearly distinguish this break. For a model with a higher force carrier to DM particle mass ratio of  $m_\phi/M_{\text{DM}} = 5 \times 10^{-5}$ , this break is indeed apparent at the higher saturation

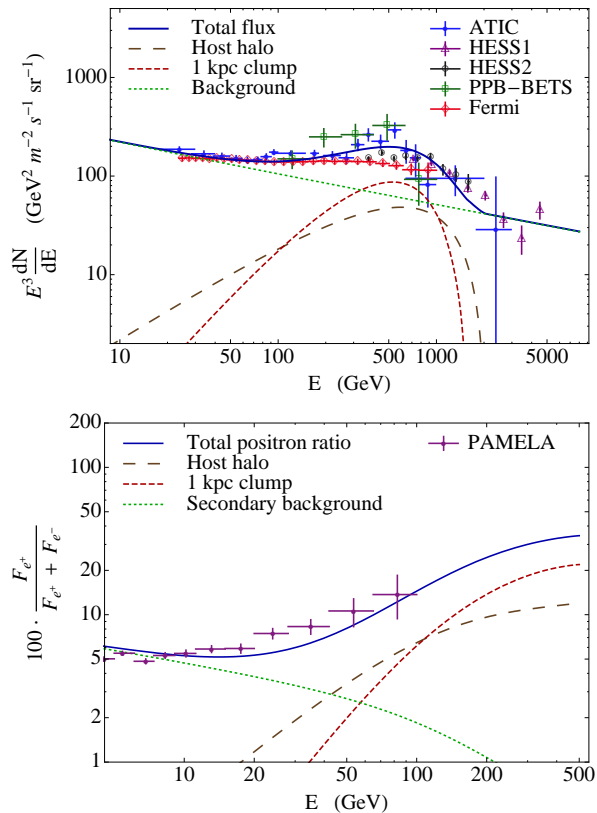


FIG. 7: Electron and positron flux from annihilating DM in the host halo plus a 1 kpc clump shown in Fig. 6. The hard spectrum of the flux from the subhalo is consistent with the ATIC bump around 600 GeV, but, in order to fit the PAMELA data, we need the softer flux from the host halo at energies  $E < 100$  GeV. We use the primary electron background  $\sim E^{-3.3}$  and secondary electron and positron backgrounds  $\sim E^{-3.6}$ . The parameters of the DM model are the same as in Fig. 6.

luminosity of  $L_{\text{sat}} = 2 \times 10^9 M_\odot^2 \text{pc}^{-3}$ . These results indicate that subhalos below the VL2 resolution limit are unlikely to either strongly enhance or suppress the likelihood of having a significant spectral feature due to an individual subhalo.

As a concrete example, we consider the electron flux from DM annihilating in a clump at a distance  $x_{\text{sub}} = 1$  kpc. We take the  $S \sim 1/v$  model with the normalization  $S_0 = S(200\text{km/s}) = 600$  and choose the

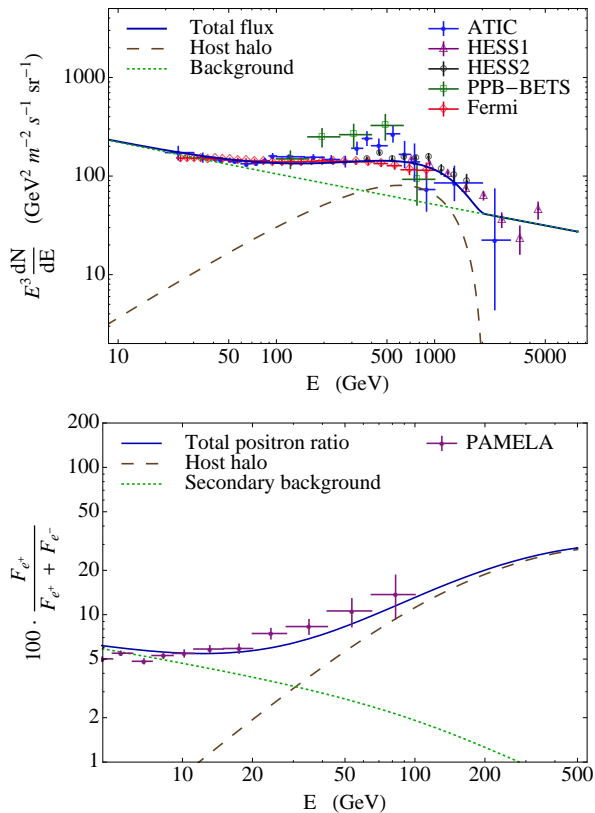


FIG. 8: The same as in Fig. 7 but without the contribution from the subhalo and with a larger local Sommerfeld enhancement in the host halo  $S_0 = 1000$  corresponding to  $\alpha = 1/30$ .

following luminosity of the DM clump

$$L_{\text{sub}} = 10^9 M_{\odot}^2 \text{pc}^{-3}. \quad (47)$$

This luminosity is equal to the total luminosity in the host halo within approximately 2 kpc from Earth.  $L_{\text{sub}}$  is about 4 times smaller than the luminosity resolved in VL2. Consequently, in the equipartition case  $s = 2$ , the probability to find a clump of DM with  $L > L_{\text{sub}}$  is around  $4 \cdot 4\% = 16\%$ . The source function for the electrons and positrons from DM annihilating in a subhalo at position  $\mathbf{x}_{\text{sub}}$  is

$$Q_{\text{sub}}(\mathbf{x}, E) = \kappa L_{\text{sub}} \delta^3(\mathbf{x} - \mathbf{x}_{\text{sub}}) Q(E). \quad (48)$$

The flux from a DM subhalo can be obtained by sub-

stituting the source  $Q_{\text{sub}}$  into the general solution (8)

$$F_{\text{sub}} = \frac{c}{4\pi} \frac{1}{b(E)} \kappa L_{\text{sub}} \int_E^{M_{\text{DM}}} dE_0 \frac{1}{(4\pi\lambda)^{3/2}} e^{-\frac{x_{\text{sub}}^2}{4\lambda}} Q(E_0). \quad (49)$$

In our example, we use the DM toy model from section III B with the annihilation chain  $2\chi \rightarrow 2\phi_1 \rightarrow 4\phi_2 \rightarrow 4e^+ + 4e^-$ . The corresponding source function  $Q_3(E)$  was presented in Eq. (31). This model can be considered as a toy model for a more realistic decay through pions or muons instead of  $\phi_2$ . If there are four pions (muons) after the decay of  $\phi_1$ , then there will be only 2 electrons and 2 positrons in the final state and the boost factor in this model should be about twice larger than the boost factor in the toy model with 4 electrons and 4 positrons in the final state.

In Fig. 6, we compare the flux from a subhalo with the flux from the host halo

$$F_{\text{host}} = \frac{c}{4\pi} \frac{1}{b(E)} \int_E^{M_{\text{DM}}} dE_0 \kappa \langle \rho_{\text{DM}}^2 S_0 \rangle Q(E_0). \quad (50)$$

Since the dependence on the host halo density profile is insignificant, we use the homogeneous DM distribution with  $\rho_{\text{DM}} = 0.3 \text{ GeV cm}^{-3}$  and  $\langle \sigma v \rangle_0 = 3 \times 10^{-26} \text{ cm}^3 \text{ s}^{-1}$ . We have chosen a local boost factor of  $S_0 = 600$  and a DM particle mass of  $M_{\text{DM}} = 2.1 \text{ TeV}$  in order to fit the ATIC and PAMELA data (see Fig. 7). Thus the flux in the presence of significant contribution from a subhalo is consistent with the ATIC and PPB-BETS data but may contradict the Fermi data if we simultaneously fit to the PAMELA positron ratio.

The flux from the host halo without subhalos is shown in Fig. 8, where we use the same model as above but increase the boost factor to  $S_0 = 900$  in order to fit the PAMELA, Fermi, and HESS points. For a smaller DM mass, one can also fit the PAMELA and ATIC data (as was shown, for instance, in [15]). Thus either the ATIC or the Fermi data can be explained by DM annihilation in the host halo for different parameters in the DM models (but not simultaneously, since ATIC and Fermi data have significant deviations from each other at energies between 300 GeV and 700 GeV). The fits of the flux from the host halo to the Fermi-LAT and PAMELA data and the corresponding ranges of

parameters for a more realistic counterpart of our toy model with the annihilation chain  $2\chi \rightarrow 2\phi_1 \rightarrow 4\mu^\pm$  can be found in [75].

## V. CONCLUSIONS

In this paper we have studied the  $e^+e^-$  flux from annihilating DM. We analyzed the dependence of the flux on the choice of DM model, on the profile of the DM halo, and on the presence of a local subhalo.

The DM models we have considered here are characterized by the mass of the DM particle  $M_{\text{DM}}$  and by the number of step  $k$  in the annihilation-decay process from DM to  $e^+e^-$ . In particular, we studied a toy model where the DM particles annihilate into two scalars that decay by a chain of  $(k - 1)$  two-body decays into electrons and positrons. In this model,  $\log \frac{M_{\text{DM}}}{E_*} \approx \frac{k-1}{2}$  and, as expected,  $F \sim E^{-2}$  for  $E \ll E_*$ . The behavior of the flux for  $E \sim E_*$  is model dependent. The spectrum has a sharper cutoff in models with fewer decay steps.

The dependence on the shape of the DM host halo is very mild, provided that the DM distribution is sufficiently smooth. For the typical DM halo profiles, such as NFW, Einasto, and Isothermal,  $\delta n \lesssim 10\%$ .

If a small number of DM subhalos contribute significantly to the DM annihilation, then the corresponding source function may have large variations and the index of the propagated  $e^+e^-$  flux will change as well. In general the index grows, i.e., the flux from a subhalo is harder than the flux from the host halo. Using the *Via Lactea II* simulation, we argue that, on average, we expect one  $M > 10^5 M_\odot$  subhalo within 3 kpc from the Earth, and the flux from such a subhalo will leave a significant imprint on the electron spectrum above  $\sim 100$  GeV, if its distance is less than  $\sim 1$  kpc. Thus, based on the *Via Lactea II* simulation, there is at least a  $\sim 4\%$  chance to observe the flux of electrons and positrons from a local DM subhalo. Extrapolating below the VL2 resolution limit, we estimate that this probability may grow to  $\sim 15\%$ .

In the presence of DM subhalos, there may be some features in the  $e^+e^-$  flux spectrum at high energies, but at low energies we should still expect the univer-

sal index  $n \approx -2$  of the DM annihilation flux. Future observations will help to distinguish between the following possibilities:

- The additional flux is dominated by a local DM clump at all energies. Then the index of the flux is not universal and, as a rule,  $n > -2$ , i.e. the flux is harder than the flux from the host halo. However, as was pointed out in [15], we need a flux with an index  $n = -2.2 \pm 0.2$  in order to fit both ATIC and PAMELA data. This problem becomes even worse if one tries to fit simultaneously the PAMELA points and rather soft Fermi/LAT spectrum. Therefore this possibility contradicts current data.
- The additional flux is dominated by a local DM clump at high energies, 100 - 1000 GeV, and by the host halo at low energies, 10 - 100 GeV. We present an example with a DM clump at 1 kpc from the Earth consistent with the ATIC and PAMELA data. However, this flux may be inconsistent with the Fermi/LAT and the HESS data. The flux from annihilating DM has an index  $n \approx -2$  at energies  $E < 100$  GeV and  $n > -2$  at energies  $100 \text{ GeV} < E < 300 \text{ GeV}$ .
- The additional flux is dominated by the host halo at all energies. For different DM models this flux can fit either PAMELA and ATIC or PAMELA and Fermi data but not both. The property that the positron ratio is fitted in both cases is a consequence of a general fact that, independently of DM model and the shape of the DM halo profile, we expect an index  $n \approx -2$  for energies much smaller than the cutoff scale  $E \ll E_*$ .

Our main conclusion is that at lower energies  $E \ll M_{\text{DM}}$ , i.e. in the PAMELA range 10 - 100 GeV for  $M_{\text{DM}} \gtrsim 1$  TeV, one should expect the flux from the DM to have a universal index  $n \approx -2$ . At higher energies, i.e., in the ATIC - Fermi range 100 - 1000 GeV, the behavior of the flux is model dependent. In the presence of a significant nearby clump of DM one should expect an ATIC-like bump in the spectrum whereas in the absence of large nearby clumps the flux should look smooth, similar to the Fermi/LAT and HESS data.

**Acknowledgments.**

The authors are thankful to J. Bovy, I. Cholis, J. Die-  
mand, L. Goodenough, J. Roberts, and N. Weiner for  
valuable discussions. This work is supported in part  
by the Russian Foundation of Basic Research under  
Grant No. RFBR 09-02-00253 (DM), by NSF Grant  
Nos. PHY-0245068 (DM) and PHY-0758032 (DM).  
MK acknowledges support from the William L. Lough-  
lin Fellowship at the Institute for Advanced Study.

- 
- [1] O. Adriani *et al.*, “Observation of an anomalous positron abundance in the cosmic radiation,” [arXiv:0810.4995 \[astro-ph\]](#).
- [2] J. Chang *et al.*, “An excess of cosmic ray electrons at energies of 300.800 GeV,” *Nature* **456** (2008) 362–365.
- [3] S. Torii *et al.*, “High-energy electron observations by PPB-BETS flight in Antarctica,” [arXiv:0809.0760 \[astro-ph\]](#).
- [4] H.E.S.S. Collaboration, F. Aharonian *et al.*, “The energy spectrum of cosmic-ray electrons at TeV energies,” *Phys. Rev. Lett.* **101** (2008) 261104, [arXiv:0811.3894 \[astro-ph\]](#).
- [5] F. Collaboration, “Measurement of the Cosmic Ray  $e^+$  plus  $e^-$  spectrum from 20 GeV to 1 TeV with the Fermi Large Area Telescope,” [arXiv:0905.0025 \[astro-ph.HE\]](#).
- [6] H. E. S. S. C. F. Aharonian, “Probing the ATIC peak in the cosmic-ray electron spectrum with H.E.S.S.,” [arXiv:0905.0105 \[astro-ph.HE\]](#).
- [7] F. A. Aharonian, A. M. Atoyan, and H. J. Voelk, “High energy electrons and positrons in cosmic rays as an indicator of the existence of a nearby cosmic tevatron,” *Astron. Astrophys.* **294** (1995) L41–L44.
- [8] L. Zhang and K. S. Cheng, “Cosmic-ray positrons from mature gamma-ray pulsars,” *Astron. Astrophys.* **368** (2001) 1063–1070.
- [9] T. Kobayashi, Y. Komori, K. Yoshida, and J. Nishimura, “The most likely sources of high energy cosmic-ray electrons in supernova remnants,” *Astrophys. J.* **601** (2004) 340–351, [arXiv:astro-ph/0308470](#).
- [10] D. Hooper, P. Blasi, and P. D. Serpico, “Pulsars as the Sources of High Energy Cosmic Ray Positrons,” *JCAP* **0901** (2009) 025, [arXiv:0810.1527 \[astro-ph\]](#).
- [11] H. Yuksel, M. D. Kistler, and T. Stanev, “TeV Gamma Rays from Geminga and the Origin of the GeV Positron Excess,” [arXiv:0810.2784 \[astro-ph\]](#).
- [12] S. Profumo, “Dissecting Pamela (and ATIC) with Occam’s Razor: existing, well-known Pulsars naturally account for the ‘anomalous’ Cosmic-Ray Electron and Positron Data,” [arXiv:0812.4457 \[astro-ph\]](#).
- [13] K. Ioka, “A Gamma-Ray Burst/Pulsar for Cosmic-Ray Positrons with a Spectral Cutoff and Line,” [arXiv:0812.4851 \[astro-ph\]](#).
- [14] N. J. Shaviv, E. Nakar, and T. Piran, “Natural explanation for the anomalous positron to electron ratio with supernova remnants as the sole cosmic ray source,” [arXiv:0902.0376 \[astro-ph.HE\]](#).
- [15] D. Malyshev, I. Cholis, and J. Gelfand, “Pulsars versus Dark Matter Interpretation of ATIC/PAMELA,” [arXiv:0903.1310 \[astro-ph.HE\]](#).
- [16] N. Kawanaka, K. Ioka, and M. M. Nojiri, “Cosmic-Ray Electron Excess from Pulsars is Spiky or Smooth?: Continuous and Multiple Electron/Positron injections,” [arXiv:0903.3782 \[astro-ph.HE\]](#).
- [17] J. Diemand *et al.*, “Clumps and streams in the local dark matter distribution,” [arXiv:0805.1244 \[astro-ph\]](#).
- [18] N. Arkani-Hamed, D. P. Finkbeiner, T. Slatyer, and N. Weiner, “A Theory of Dark Matter,” (2008) , [arXiv:0810.0713 \[hep-ph\]](#).
- [19] M. Lattanzi and J. I. Silk, “Can the WIMP annihilation boost factor be boosted by the Sommerfeld enhancement?,” [arXiv:0812.0360 \[astro-ph\]](#).
- [20] M. Cirelli, R. Franceschini, and A. Strumia, “Minimal Dark Matter predictions for galactic positrons, anti-protons, photons,” *Nucl. Phys.* **B800** (2008) 204–220, [arXiv:0802.3378 \[hep-ph\]](#).
- [21] M. Kuhlen, P. Madau, and J. Silk, “Exploring the dark sector with Milky Way substructure,” submitted to *Science*.
- [22] S. Dimopoulos, G. F. Giudice, and A. Pomarol, “Dark matter in theories of gauge-mediated supersymmetry breaking,” *Phys. Lett.* **B389** (1996) 37–42, [arXiv:hep-ph/9607225](#).
- [23] L. Bergstrom, T. Bringmann, and J. Edsjo, “New Positron Spectral Features from Supersymmetric Dark Matter - a Way to Explain the PAMELA Data?,” *Phys. Rev.* **D77** (2008) 103520, [arXiv:0808.3725 \[astro-ph\]](#).
- [24] R. Allahverdi, B. Dutta, K. Richardson-McDaniel, and Y. Santoso, “A Supersymmetric B - L Dark Matter Model and the Observed Anomalies in the Cosmic Rays,” [arXiv:0812.2196 \[hep-ph\]](#).
- [25] T. Banks and J.-F. Fortin, “A Pyramid Scheme for Particle Physics,” [arXiv:0901.3578 \[hep-ph\]](#).

- [26] C. Cheung, J. T. Ruderman, L.-T. Wang, and I. Yavin, “Kinetic Mixing as the Origin of Light Dark Scales,” [arXiv:0902.3246 \[hep-ph\]](#).
- [27] A. Katz and R. Sundrum, “Breaking the Dark Force,” [arXiv:0902.3271 \[hep-ph\]](#).
- [28] G. Servant and T. M. P. Tait, “Is the lightest Kaluza-Klein particle a viable dark matter candidate?,” *Nucl. Phys.* **B650** (2003) 391–419, [arXiv:hep-ph/0206071](#).
- [29] H.-C. Cheng, J. L. Feng, and K. T. Matchev, “Kaluza-Klein dark matter,” *Phys. Rev. Lett.* **89** (2002) 211301, [arXiv:hep-ph/0207125](#).
- [30] D. Hooper and K. Zurek, “The PAMELA and ATIC Signals From Kaluza-Klein Dark Matter,” [arXiv:0902.0593 \[hep-ph\]](#).
- [31] I. Cholis, L. Goodenough, and N. Weiner, “High Energy Positrons and the WMAP Haze from Exciting Dark Matter,” [arXiv:0802.2922 \[astro-ph\]](#).
- [32] I. Cholis, L. Goodenough, D. Hooper, M. Simet, and N. Weiner, “High Energy Positrons From Annihilating Dark Matter,” [arXiv:0809.1683 \[hep-ph\]](#).
- [33] M. Cirelli, M. Kadastik, M. Raidal, and A. Strumia, “Model-independent implications of the  $e^+$ ,  $e^-$ , anti-proton cosmic ray spectra on properties of Dark Matter,” [arXiv:0809.2409 \[hep-ph\]](#).
- [34] I. Cholis, D. P. Finkbeiner, L. Goodenough, and N. Weiner, “The PAMELA Positron Excess from Annihilations into a Light Boson,” [arXiv:0810.5344 \[astro-ph\]](#).
- [35] E. Ponton and L. Randall, “TeV Scale Singlet Dark Matter,” [arXiv:0811.1029 \[hep-ph\]](#).
- [36] I. Cholis, G. Dobler, D. P. Finkbeiner, L. Goodenough, and N. Weiner, “The Case for a 700+ GeV WIMP: Cosmic Ray Spectra from ATIC and PAMELA,” [arXiv:0811.3641 \[astro-ph\]](#).
- [37] D. J. Phalen, A. Pierce, and N. Weiner, “Cosmic Ray Positrons from Annihilations into a New, Heavy Lepton,” [arXiv:0901.3165 \[hep-ph\]](#).
- [38] D. Hooper, “TASI 2008 Lectures on Dark Matter,” [arXiv:0901.4090 \[hep-ph\]](#).
- [39] L. Bergstrom, “Dark Matter Candidates,” [arXiv:0903.4849 \[hep-ph\]](#).
- [40] C.-R. Chen, K. Hamaguchi, M. M. Nojiri, F. Takahashi, and S. Torii, “Dark Matter Model Selection and the ATIC/PPB-BETS anomaly,” [arXiv:0812.4200 \[astro-ph\]](#).
- [41] P. Meade, M. Papucci, and T. Volansky, “Dark Matter Sees The Light,” [arXiv:0901.2925 \[hep-ph\]](#).
- [42] J. Mardon, Y. Nomura, D. Stolarski, and J. Thaler, “Dark Matter Signals from Cascade Annihilations,” [arXiv:0901.2926 \[hep-ph\]](#).
- [43] M. Kuhlen, J. Diemand, and P. Madau, “The Dark Matter Annihilation Signal from Galactic Substructure: Predictions for GLAST,” [arXiv:0805.4416 \[astro-ph\]](#).
- [44] P. Madau *et al.*, “Fossil remnants of reionization in the halo of the Milky Way,” [arXiv:0810.3712 \[astro-ph\]](#).
- [45] P. Brun, T. Delahaye, J. Diemand, S. Profumo, and P. Salati, “The cosmic ray lepton puzzle in the light of cosmological N-body simulations,” [arXiv:0904.0812 \[astro-ph.HE\]](#).
- [46] M. Pohl, “Cosmic-ray electron signatures of dark matter,” [arXiv:0812.1174 \[astro-ph\]](#).
- [47] D. Hooper, A. Stebbins, and K. M. Zurek, “The PAMELA and ATIC Excesses From a Nearby Clump of Neutralino Dark Matter,” [arXiv:0812.3202 \[hep-ph\]](#).
- [48] I. Cholis *et al.*, *work in progress*.
- [49] V. L. Ginzburg and S. I. Syrovatskii, *The Origin of Cosmic Rays*. Pergamon, Oxford, 1964.
- [50] M. S. Longair, *High-energy astrophysics*. Cambridge University Press, 1992.
- [51] T. A. Porter and A. W. Strong, “A new estimate of the Galactic interstellar radiation field between 0.1 microns and 1000 microns,” [arXiv:astro-ph/0507119](#).
- [52] D. Maurin, F. Donato, R. Taillet, and P. Salati, “Cosmic Rays below  $Z=30$  in a diffusion model: new constraints on propagation parameters,” *Astrophys. J.* **555** (2001) 585–596, [arXiv:astro-ph/0101231](#).
- [53] T. Delahaye, R. Lineros, F. Donato, N. Fornengo, and P. Salati, “Positrons from dark matter annihilation in the galactic halo: theoretical uncertainties,” *Phys. Rev.* **D77** (2008) 063527, [arXiv:0712.2312 \[astro-ph\]](#).
- [54] A. W. Strong, I. V. Moskalenko, and V. S. Ptuskin, “Cosmic-ray propagation and interactions in the Galaxy,” *Ann. Rev. Nucl. Part. Sci.* **57** (2007) 285–327, [arXiv:astro-ph/0701517](#).
- [55] S. I. Syrovatskii, “The Distribution of Relativistic Electrons in the Galaxy and the Spectrum of Synchrotron Radio Emission,” *Astr. Zh.* **36** (1959) 17.



- [56] J. Diemand, B. Moore, and J. Stadel, “Velocity and spatial biases in CDM subhalo distributions,” *Mon. Not. Roy. Astron. Soc.* **352** (2004) 535, [arXiv:astro-ph/0402160](#).
- [57] M. Hoeft, J. P. Mucket, and S. Gottlober, “Velocity dispersion profile in dark matter halos,” *Astrophys. J.* **602** (2004) 162–169, [arXiv:astro-ph/0311083](#).
- [58] W. Dehnen and D. McLaughlin, “Dynamical insight into dark-matter haloes,” *Mon. Not. Roy. Astron. Soc.* **363** (2005) 1057–1068, [arXiv:astro-ph/0506528](#).
- [59] B. Robertson and A. Zentner, “Dark Matter Annihilation Rates with Velocity-Dependent Annihilation Cross Sections,” [arXiv:0902.0362 \[astro-ph.CO\]](#).
- [60] S. Tremaine *et al.*, “A Family of Models for Spherical Stellar Systems,” *Astron. J.* **107** (1994) 634, [arXiv:astro-ph/9309044](#).
- [61] M. Pospelov and A. Ritz, “Astrophysical Signatures of Secluded Dark Matter,” *Phys. Lett.* **B671** (2009) 391–397, [arXiv:0810.1502 \[hep-ph\]](#).
- [62] V. Barger, Y. Gao, W. Y. Keung, D. Marfatia, and G. Shaughnessy, “Dark matter and pulsar signals for Fermi LAT, PAMELA, ATIC, HESS and WMAP data,” [arXiv:0904.2001 \[hep-ph\]](#).
- [63] J. F. Beacom, N. F. Bell, and G. D. Mack, “General upper bound on the dark matter total annihilation cross section,” *Phys. Rev. Lett.* **99** (2007) 231301, [arXiv:astro-ph/0608090](#).
- [64] J. Liu, P.-f. Yin, and S.-h. Zhu, “Prospects for Detecting Neutrino Signals from Annihilating/Decaying Dark Matter to Account for the PAMELA and ATIC results,” [arXiv:0812.0964 \[astro-ph\]](#).
- [65] I. V. Moskalenko and A. W. Strong, “Production and propagation of cosmic-ray positrons and electrons,” *Astrophys. J.* **493** (1998) 694–707, [arXiv:astro-ph/9710124](#).
- [66] J. F. Navarro, C. S. Frenk, and S. D. M. White, “A Universal Density Profile from Hierarchical Clustering,” *Astrophys. J.* **490** (1997) 493–508, [arXiv:astro-ph/9611107](#).
- [67] J. F. Navarro *et al.*, “The Inner Structure of LambdaCDM Halos III: Universality and Asymptotic Slopes,” *Mon. Not. Roy. Astron. Soc.* **349** (2004) 1039, [arXiv:astro-ph/0311231](#).
- [68] J. N. Bahcall and R. M. Soneira, “The Universe at faint magnetitudes. 2. Models for the predicted star counts,” *Astrophys. J. Suppl.* **44** (1980) 73–110.
- [69] M. Kamionkowski and A. Kinkhabwala, “Galactic halo models and particle dark matter detection,” *Phys. Rev.* **D57** (1998) 3256–3263, [arXiv:hep-ph/9710337](#).
- [70] D. Hooper and J. Silk, “Searching for dark matter with future cosmic positron experiments,” *Phys. Rev.* **D71** (2005) 083503, [arXiv:hep-ph/0409104](#).
- [71] V. Springel *et al.*, “The Aquarius Project: the subhalos of galactic halos,” [arXiv:0809.0898 \[astro-ph\]](#).
- [72] T. Goerdt, O. Y. Gnedin, B. Moore, J. Diemand, and J. Stadel, “The survival and disruption of CDM micro-haloes: implications for direct and indirect detection experiments,” *Mon. Not. Roy. Astron. Soc.* **375** (2007) 191–198, [arXiv:astro-ph/0608495](#).
- [73] S. Profumo, K. Sigurdson, and M. Kamionkowski, “What mass are the smallest protohalos?,” *Phys. Rev. Lett.* **97** (2006) 031301, [arXiv:astro-ph/0603373](#).
- [74] T. Bringmann, “Particle Models and the Small-Scale Structure of Dark Matter,” [arXiv:0903.0189 \[astro-ph.CO\]](#).
- [75] L. Bergstrom, J. Edsjo, and G. Zaharijas, “Dark matter interpretation of recent electron and positron data,” [arXiv:0905.0333 \[astro-ph.HE\]](#).